Lab on a Chip

PAPER

View Article Online
View Journal | View Issue

Cite this: *Lab Chip*, 2021, **21**, 4144

Non-invasive and label-free identification of human natural killer cell subclasses by biophysical single-cell features in microfluidic flow†

David Dannhauser, [a] Domenico Rossi, [b] Anna Teresa Palatucci,[c] Valentina Rubino,[d] Flavia Carriero,[d] Giuseppina Ruggiero,[d] Mimmo Ripaldi,[e] Mario Toriello,[e] Giovanna Maisto,[e] Paolo Antonio Netti,[ab] Giuseppe Terrazzano[c] and Filippo Causa *[a]

Received 21st July 2021,
Accepted 2nd September 2021

DOI: 10.1039/d1lc00651g

rsc.li/loc

Natural killer (NK) cells are indicated as favorite candidates for innovative therapeutic treatment and are divided into two subclasses: immature regulatory NK CD56^{bright} and mature cytotoxic NK CD56^{dim}. Therefore, the ability to discriminate CD56^{dim} from CD56^{bright} could be very useful because of their higher cytotoxicity. Nowadays, NK cell classification is routinely performed by cytometric analysis based on surface receptor expression. Here, we present an in-flow, label-free and non-invasive biophysical analysis of NK cells through a combination of light scattering and machine learning (ML) for NK cell subclass classification. In this respect, to identify relevant biophysical cell features, we stimulated NK cells with interleukine-15 inducing a subclass transition from CD56^{bright} to CD56^{dim}. We trained our ML algorithm with sorted NK cell subclasses (≥86% accuracy). Next, we applied our NK cell classification algorithm to cells stimulated over time, to investigate the transition of CD56^{bright} to CD56^{dim} and their biophysical feature changes. Finally, we tested our approach on several proband samples, highlighting the potential of our measurement approach. We show a label-free way for the robust identification of NK cell subclasses based on biophysical features, which can be applied in both cell biology and cell therapy.

Introduction

Natural killer (NK) cells are physiologically involved in the immune response against viruses, intra-cellular bacteria, parasites, and malignant cells. In addition to cytotoxic activity, NK cells mediate a variety of homeostatic effects by producing cytokines.[1–4] Although long described, the details of the functional characteristics of NK cells have long been a mystery. They are a specific lymphocyte type, expressing several receptors.[5] In this regard, NK cells do not express T- nor B-lymphocyte cell receptors and the activation mechanism of their functions is not restricted to antigen presentation by major histocompatibility complex (MHC) proteins.[6] However, since NK cells were identified, in the 1970s, they immediately attracted great interest in biology and in medical applications.[7] Nowadays, we know that NK cells have infiltrating capability, used to migrate in tumoral tissue to promote their high cytotoxic activity.[8–10] We also know that two main NK cell functional subclasses exist, and they can be recognized, basing on the cell surface expression of the CD56 marker:[11] CD56^{bright} (high CD56 expression) and CD56^{dim} (low CD56 expression).[12] In more detail, CD56^{bright} NK cells produce cytokines, but lack in cytotoxicity, while CD56^{dim} NK cells have a primary role in cytotoxic function.[13] It is also known that CD56^{bright} NK cells are immature and represent the minority (~10%) of peripheral blood circulant NK cells.[14–16] Beyond that, other classifications of NK cells have arisen over the years, also identifying peripheral subclasses or infiltrating types.[17–20] The more the knowledge on NK became complete, the more their immunological importance became clear, since a new therapeutic strategy has been recently hypothesized by selecting the best performing cytotoxic NK cells to re-infuse them in patients and maximize the effect of antitumor therapies.[21–27] For this reason, recently, research studies started to focus on the CD56^{dim} subclass, which shows higher cytotoxic potential. For

[a] *Interdisciplinary Research Centre on Biomaterials (CRIB) and Dipartimento di Ingegneria Chimica, dei Materiali e della Produzione Industriale, Università degli Studi di Napoli "Federico II", Piazzale Tecchio 80, 80125 Naples, Italy. E-mail: causa@unina.it*

[b] *Center for Advanced Biomaterials for Healthcare@CRIB, Istituto Italiano di Tecnologia, Largo Barsanti e Matteucci 53, 80125 Naples, Italy*

[c] *Dipartimento di Scienze (DiS), Università della Basilicata, Via dell'Ateneo Lucano 10, 85100 Potenza, Italy*

[d] *Dipartimento di Scienze Mediche Traslazionali, Università degli Studi di Napoli "Federico II", Naples, Italy*

[e] *Dipartimento Oncologia AORN Santobono Pausilipon Hospital, Via Posillipo, 226, 80123, Naples, Italy*

† Electronic supplementary information (ESI) available. See DOI: 10.1039/d1lc00651g

instance, interleukin 15 (IL-15) results in an enhancement of cytotoxic activities, *i.e.*, a variation of nucleus-ratio in favour of the cytosol compartment.[28–32] In particular, a high cytotoxic activity of NK cells is of significant interest for therapies to minimize the effects of graft *versus* host diseases (GvHDs) in bone marrow transplants.

However, NK cell subclasses are distinguished by immunofluorescence approaches, based on a combination of monoclonal antibodies and flow cytometry.[33,34] The drawbacks and limitations of flow cytometry are instrumentation and service costs, as well as the high number of fluorescent antibody types, which are in general expensive, and suffer from variability during their production processes. Furthermore, for the execution of immunofluorescence techniques, specialized operators are required to correctly interpret the obtained results.[35–37] Moreover, monoclonal antibodies against cell surface molecules may interfere with cell functions. Therefore, methods to preserve the integrity of cell functions are desirable when cells are used for therapeutic purposes. Thus, although molecular characterization by flow cytometry represents the gold standard technique for the evaluation of cell classes, there is evidence in the literature that morphological cell parameters reveal many characteristics of cells.[38–45] For instance, Walsh *et al.* and Do-Hyun Lee *et al.* discovered that cells can be recognized and classified based on their autofluorescence.[46,47] Nassar *et al.* used bright-field and fluorescence imaging of white blood cells and classified them, taking advantage of machine learning,[48] while Isozaki[49] and Kim[50] took advantage of artificial intelligence for automatic recognition of cells by acquiring their shape, structure and substructure. Another interesting application in this field is digital holographic microscopy,[51–53] which permits a very detailed reconstruction of cell shape, but requires a high computational cost and long time of analysis. Acquisition of detailed morphological aspects of cells, whatever the used technique, is a powerful possibility, because it supplies early information on the cell state, which could escape to cytometric analysis, like substructure anomalies, or the nucleus state (reflecting DNA organization). Recently, a simple label-free classification of peripheral human blood stream cells using a self-built small angle light scattering technique associated with a viscoelastic microfluidic cell alignment approach was presented.[54] In detail, morphological features of different human cell classes have been measured: red blood cells,[55] lymphocyte subclasses,[56,57] and monocytes.[58] No examples of NK cell identification based on such a paradigm exist in the literature. Here, we present a novel approach to classify human NK cell subclasses exclusively based on their morphological and biophysical aspects obtained *via* an in-flow light scattering approach (Fig. 1). We trained a machine learning (ML) algorithm on sorted NK cell subclasses, extracting their biophysical cell features (diameter, nucleus ratio, optical density). Based on such input, we applied the obtained classification algorithm on physiological NK cells as well as on mobilized NK cells. Later, NK cells were utilized to investigate biophysical cell feature changes based on the classification accuracy. Therefore, we measured mobilized NK cells after IL-15 stimulation and followed the transition from $CD56^{bright}$ to $CD56^{dim}$. However, the generated classification algorithm is applied to NK suspensions obtained from four different probands to reveal *via* scattering measurements the $CD56^{bright}$ *versus* $CD56^{dim}$ predictions and associated score values. Our measurement approach allows the distinct classification and selection of cytotoxic NK cells and strengthens the actual knowledge on these fundamental classes of cells. More importantly, we show a potential way to properly identify mobilized NK cells destined for therapeutic purposes, which could be done by implementing appropriate

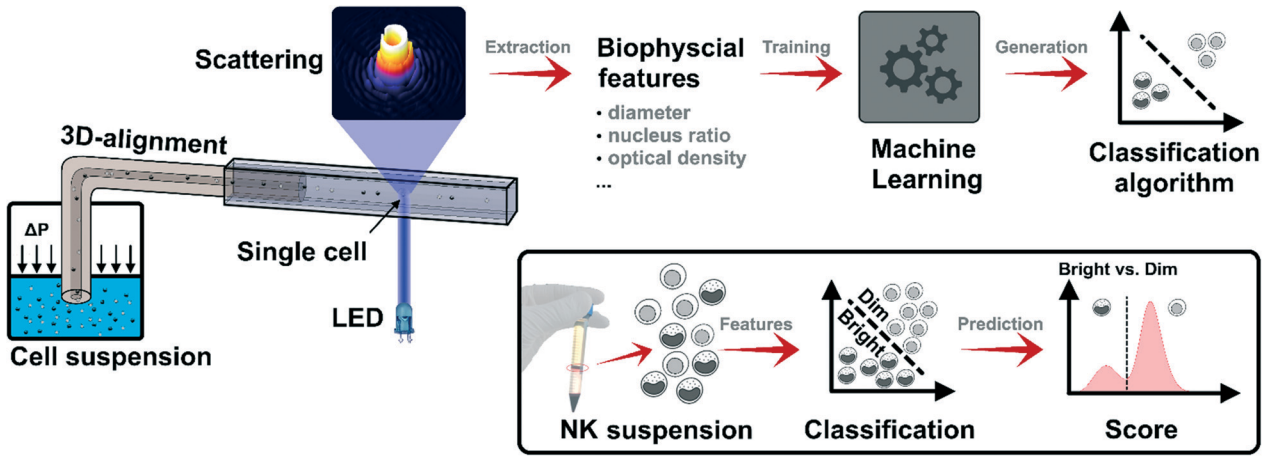

Fig. 1 Overview of the experimental approach. A cell suspension is 3D-aligned in a round shaped channel before entering a square shaped readout channel, where single cell investigation takes place. From the obtained scattering pattern, biophysical cell features are extracted and used for training of the ML classification algorithm. The generated classification algorithm is applied to NK cell suspensions obtained from a patient to reveal *via* scattering measurements the $CD56^{bright}$ *versus* $CD56^{dim}$ predictions and associated score values. Afterwards, the obtained $CD56^{dim}$ could be potentially used for re-infusion in a patient.

sterility protocols to the whole approach, potentially used for re-infusion into patients.

Materials and methods

Experimental protocols

We investigated peripheral blood mononuclear cells (PBMCs), which were obtained from four healthy donor buffy coats obtained from the blood bank of the medical school of the Federico II University of Naples (Italy). At the time of blood donation, each donor signed an informed consent (model no. 5526 of Azienda Ospedaliera Universitaria "FEDERICO II", Naples, Italy) in which it is specified that waste parts of the blood (buffy coats), not useful for the medical–therapeutic purposes of blood donation, could be used for scientific research purposes. All the experiments were performed and analysed anonymously, without any biographical reference to the donors.

PBMCs were collected using standard density gradient centrifugation, with some adaptation to reduce platelet contaminations.[59] Briefly, a blood sample was gently layered on an equal volume of density gradient fluid (Ficoll) and centrifuged at $300\vec{g}$ for 45 minutes (without brake). The PBMC ring stratified at the interface between Ficoll and plasma was collected using a Pasteur pipette and washed twice with RBC lysis solution to eliminate possible erythrocyte contaminations of the sample.[60,61] After separation, the PBMCs were washed and incubated in full medium – 5 ml of RPMI (Euroclone), 10% FBS (Sigma Aldrich), and 1% pen–strep (Sigma Aldrich) – in a horizontally placed plastic flask, for two hours at 37 °C and 5% CO_2 to remove adherent cells.

Multiparametric flow cytometry was used to evaluate the percentage of T-lymphocytes ($CD3^+$ $CD56^-$) and NK cells ($CD3^-$ $CD56^+$) in the whole PBMC cell population. In particular, FITC anti-human CD3 (BD Pharmingen, UCHT1 clone) and APC anti-human CD56 (BD Biosciences, NCAM16.2 clone) monoclonal antibodies were used and analysed using an Attune NxT (Life Technologies, Thermo Fisher, Italy) cytometer apparatus.[62] To separate the $CD56^{bright}$ and $CD56^{dim}$ NK cell subclasses, a subsequent high-performance cell sorting was performed (BD FACS-Jazz, BD Bioscience, Sorting Facility of Istituto per l'Endocrinologia e l'Oncologia Sperimentale "G. Salvatore", Consiglio Nazionale delle Ricerche, Naples 80131, Italy), after staining with APC anti-human CD56 (BD Biosciences, NCAM16.2 clone) monoclonal antibodies.[62]

A second investigation was performed on a sample of mobilized NK cells obtained from the Santobono-Pausilipon Hospital, Department of Pediatric Hemato-Oncology, where PBMCs of a healthy donor were mobilized with 10 μg kg^{-1} G-CSF. The sample was taken after obtaining informed consent from the donor in accordance with relevant guidelines and regulations. The experimental protocol was approved by a licensing committee (EU clinical trial register – EudraCT Number: 2007-004270-43). The donor gave informed consent to publish identifying information. Out from such mobilized PBMCs, NK cell subclasses were selected through continuous immunomagnetic selection. The mobilized NK cells were stimulated with 100 ng ml^{-1} IL-15 and the morphometric evolution over experiment time was investigated. Therefore, we incubated cells in a T25 flask (1×10^6 cells) in full medium at controlled ambience (37 °C, 5% CO_2) for up to 120 hours. We performed measurements at six subsequent time steps: 0 h, 24 h, 48 h, 72 h, 96 h and 120 h. At each step, we collected 1–3 ml of sample volume according to the different time steps (~150 000 cells at each time step) and added fresh medium equivalent to the undrawn one. The collected sample was centrifuged at $200\vec{g}$ for 10 minutes, the supernatant was discarded, and the remaining cell pellet was resuspended in viscoelastic cell alignment medium.

Microfluidic device and cell alignment

Measurements were performed with a microfluidic device, composed of a supporting geometry fabricated with a 3D printer (Objet30 pro, Stratasys) and a series of glass channels. Briefly, a round shaped channel (TSP050375, Molex) – where 3D alignment of cells takes place – is inserted in a square shaped readout channel (8240, Vitrocom) – where single cell investigation takes place – which permits the precise inflow optical readout of cells. Cells are immersed in an alignment medium, consisting of a highly biocompatible viscoelastic polymer (polyethylene oxide, PEO M_W = 4 MDa, Sigma Aldrich) diluted in phosphate-buffered saline (PBS, Sigma Aldrich) at 0.4 wt%. Thanks to the resulting fluid properties, generated by viscoelastic fluid forces, cells are aligned to the centreline of the round shaped channel and subsequently remain aligned in the centreline of the microfluidic readout channel.[62,63] Note that fluid forces have been chosen to prevent cell deformation effects, while ensuring sufficient cell alignment. In more detail, one end of the round shaped channel is immersed in the cell sample: by applying a certain pressure on the sample, the cell medium is pushed through the channel and enter the microfluidic device. Cell alignment to the channel centreline is achieved if the following relationships of Θ is satisfied:

$$\Theta = 3Wi\beta^2 \frac{L}{2R} > -\ln(3.5\beta),$$

with $Wi = 2\lambda\bar{U}/2R$, where λ is the relaxation time (0.197 ms) of the viscoelastic fluid, $\bar{U}$ is the average fluid velocity (1496 μm s^{-1}), R is the channel radius (25 μm), $\beta = r_1/R$, a non-dimensional geometrical channel parameter, with r_1 being the cell radius, and L is the channel length (0.35 m).[62,64] The subsequent readout channel allows precise single cell analysis due to its square shape of 400 × 400 μm and preserved centreline alignment. To assure continuity between the alignment and readout channel, the alignment section is collinearly inserted in the readout section and sealed with a soft ferrule (UP-N-123-03X, IDEX). At the end of the readout channel, cells are recovered for further studies.

Light scattering and machine learning approach

We used a measurement approach, which can obtain precise single cell scattering information in a continuous angular range from 2° up to 30°, with an angular resolution of 0.1°. Briefly, cells flowing in the readout channel pass through a collimated laser beam (λ = 450 nm), and the scattered light is collected and mapped on a camera sensor (ORCA Flash 4.0, Hamamatsu). The hereby-obtained scattering signatures are processed to obtain a light-scattering profile (LSP). The LSP is used to retrieve the biophysical features of each single NK cell. In more detail, collected LSPs are matched with a look-up table (≥330 000 curves) of previously calculated theoretical scattering profiles to retrieve biophysical cell features and to distinguish morphological properties within the sub-micrometric range. More detailed information about the LSP matching is shown elsewhere.[54,65]

We prepared cell samples of approximately 1.25×10^5 cells per mL to ensure a throughput rate of ~2 cells per s passing through the readout laser beam. Please note that the sample concentration and fluid velocities were optimized to reduce possible cell–cell interactions and cell deformation effects. The maximum throughput performance of the actual measurement approach is ~50 cells per s. However, the ML approach was implemented with the commercial software MATLAB (R2020b, MathWorks) to classify $CD56^{bright}$ cells from $CD56^{dim}$ cells, as well as the main subclasses of PBMCs based on biophysical features retrieved from the experimental scattering patterns. For $CD56^{bright}$ *versus* $CD56^{dim}$ identification, the ML makes a binary classification and associates the prediction score, which allows interpretation of the classification accuracy. Note that a high score value indicates a high cell classification accuracy. The ML results are shown in a 2 × 2 matrix, with the following values: TPR, true positive rate and FNR, false negative rate *versus* $CD56^{bright}$ and $CD56^{dim}$ input data.

Vitality tests

Before and after each cell measurement, a small cell fraction was observed with an inverted bright-field microscope (100× objective, X81, Olympus), to check their morphological aspects, and to verify the absence of significant membrane damage. In addition, we estimate the rate of cell death (20× objective, BX53, Olympus), performing a 'Trypan blue' test. Moreover, cells were observed with a confocal microscope (63× objective, LSM 710, Zeiss) to investigate cell structural changes after IL-15 stimulations over time. In such a case, cells were marked with vital stains – Hoechst for the nucleus and CellTracker for the cytosol.

Results and discussion

For a successful application of ML for NK cell subclass classification, we first performed the training step on sorted $CD56^{dim}$ and $CD56^{bright}$ NK cell subclasses. Hereby, cells were isolated using a high-performance monoclonal antibody cell sorting approach obtaining a purity ≥96% for sorted cell populations. In this regard, the $CD56^{dim}$ and $CD56^{bright}$ NK cell subclasses were purified starting from PBMCs gated on the lymphocyte region (R1) and subsequently separated by a flow cytometry gating strategy for the exclusive positivity to the CD56 marker, in terms of $CD56^{dim}$ (R2) and $CD56^{bright}$ (R3) fluorescence intensity (ESI† Fig. S5). Afterwards, cells were separately analysed with our microfluidic measurement approach. In more detail, we performed microfluidic measurements using a viscoelastic sample medium, which ensured precise 3D-alignment of single target cells to the incident laser beam. Before each measurement, we checked the cell integrity and vitality *via* bright-field microscopy observations and 'Trypan blue' tests (ESI,† Fig. S3 and S4 and Table S5). Cells appeared to be round shaped and with no visible membrane damage. Note that NK cells are circulant cells, generally not adhering to surfaces;[66] therefore, we considered cell roundness as an indicator for cell vitality.[67] Also, the viscoelastic medium used for cell alignment does not induce any significant osmotic pressure changes on investigated cells, and therefore, it does not significantly affect the cell vitality during our measurement time.[55] As a confirmation, bright-field microscopy observations were performed after cell measurements with the same results.

Our measurement approach retrieves four biophysical single cell features: cell diameter (D), refractive indices of the nucleus (RI_N) and cytosol (RI_C), and nucleus over cytosol ratio (N/C-ratio). D is a direct measure of cell dimensions, at submicrometric precision, and it infers that the analysed cells are spherical. RI_N and RI_C indicate the optical density of the corresponding cell compartments, the nucleus and cytosol. In more detail, RI_N significantly depends on the chromatin organization in a cell nucleus,[68] which is known to vary during cell life,[69] spanning from active transcription (high RI_N) to resting state (low RI_N). On the other hand, RI_C correlates with the presence of components in the cell cytosol, such as proteins and granules, or the re-organization of the cytoskeleton. Finally, the N/C-ratio relates the nucleus and overall dimensions of a cell, which is known to be a fundamental parameter for cell investigation, useful to classifying cells and to evaluating cell transformations.

Fig. 2a shows 3D scatter plots of biophysical cell features for the $CD56^{bright}$ *versus* $CD56^{dim}$ NK cell subclasses, which are used as input to train our ML algorithm. We used a quadratic support vector machine (SVM) classifier with one neighbour, the Euclidean metric distance and equal distance weights. In addition, we applied a box constraint level of 0.1 and a kernel scale of 1, reducing the penalty imposed on margin-violating observations, and, therefore, preventing overfitting of our test data. Indeed, the quadratic SVM was found to be the most suitable algorithm according to speed and accuracy (training time = 0.5 s with *circa* 30 000 observations per s and a total misclassification cost = 45). We repeated the classification five times resulting in an average prediction accuracy of 86.4%. Other classifiers resulted in lower performances: the linear SVM trained classifier showed

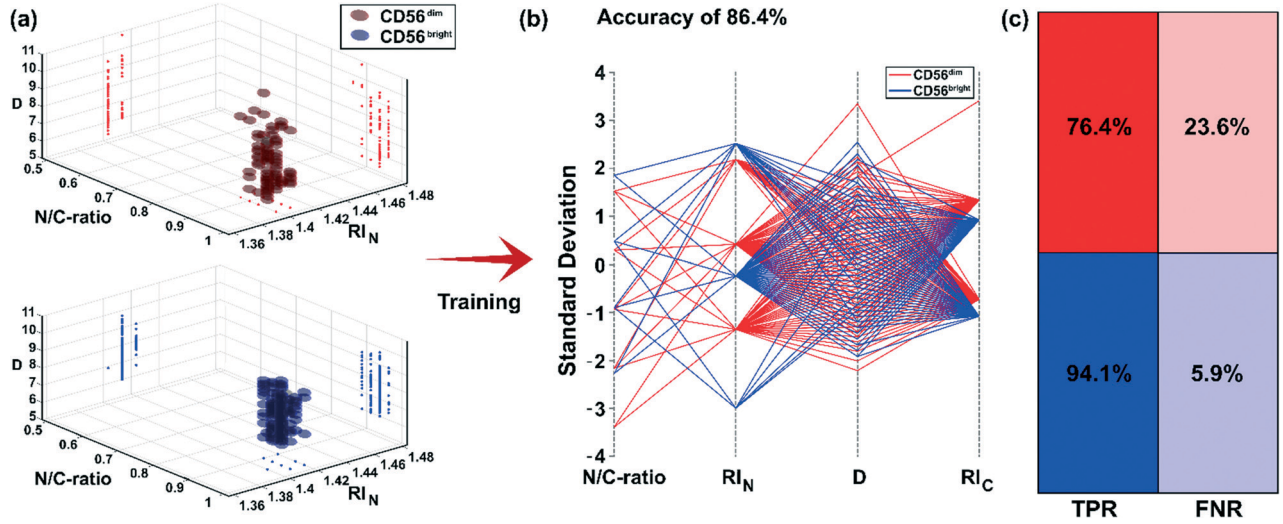

Fig. 2 Training of the ML classifier with CD56^{bright} and CD56^{dim} NK cell data from probands 3 and 4. (a) CD56^{bright} and CD56^{dim} NK cells from both probands (N = 188 and 144 for CD56^{bright} and CD56^{dim}, respectively) were measured with the light scattering apparatus. (b) Scattering outcomes are used as input for the NK cell classifier (quadratic SVM). The parallel coordinate plots indicate the correlation between the four investigated biophysical cell features, showing an overall accuracy of 86.4%. (c) ML result matrix shows a better classification accuracy for CD56^{bright} cells (true positive rate (TPR), false negative rate (FNR)).

an accuracy of 84.3%, fine K nearest neighbour (KNN) 81.6% and medium tree 86.1%. The parallel coordinate plots in Fig. 2b highlight the correlation between the four extracted biophysical cell features (each biophysical cell feature is represented by a vertical axis). The used classifier showed a TPR (or sensitivity) for CD56^{bright} cells of 94.1% and for CD56^{dim} cells of 76.4% (see Fig. 2c, ESI† Fig. S1 and Table S1). The results indicate that our ML classifier (NK cell classifier) has a better sensitivity in classifying CD56^{bright} cells compared to CD56^{dim} cells, due to the significantly different RI_N values. Since RI_N correlates with the optical density of the nucleus compartment, we infer that the chromatin state of CD56^{bright} subclasses, presumably in its active state, could be responsible for such a biophysical feature rising.[70]

Afterwards, we used mobilized NK cells, which were withdrawn from a healthy subject, who was treated with G-CSF for a bone marrow transplant of a paediatric leukemic

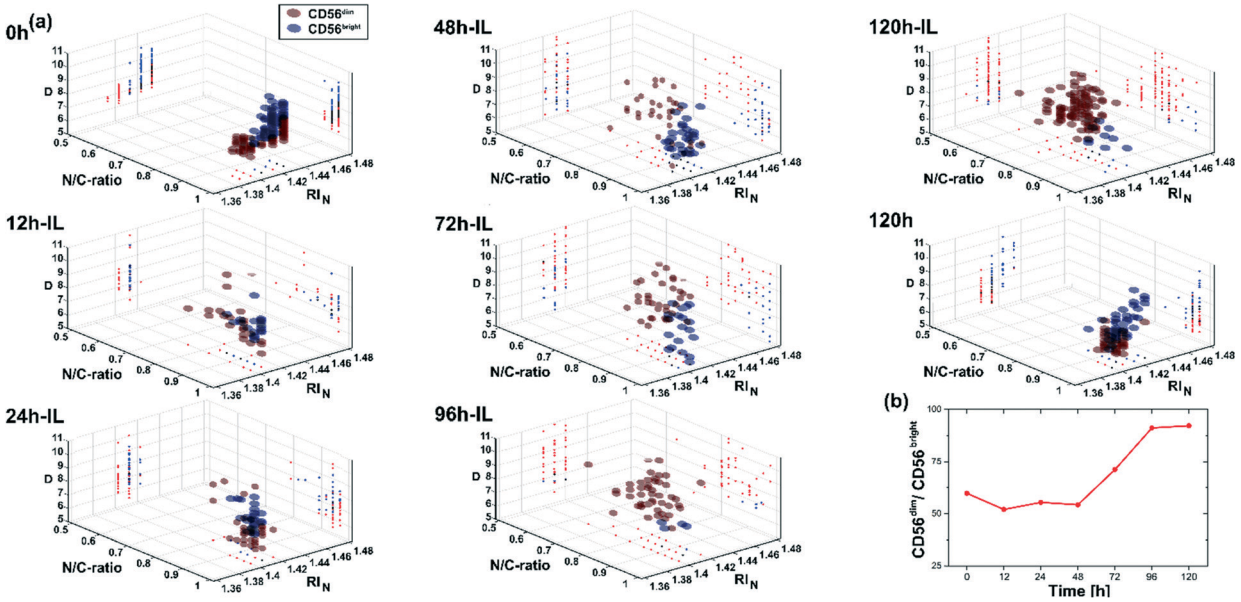

Fig. 3 IL-15 investigation of NK cells over time (0–120 h). Cells were analyzed with the light scattering measurement approach and the previously trained NK classifier was applied. (a) 3D-scatter plots show the NK subclass predictions for different biophysical cell features. Analyzed cell number = 286, 50, 74, 70, 66, 57, 129 and 97 for time 0 h, 12 h-IL, 24 h-IL, 48 h-IL, 72 h-IL, 96 h-IL, 120 h-IL and 120 h, respectively. (b) CD56^{dim} over CD56^{bright} outcome shown for stimulated cells (0 h to 120 h–IL). Note that 120 h (without IL-15) is not plotted.

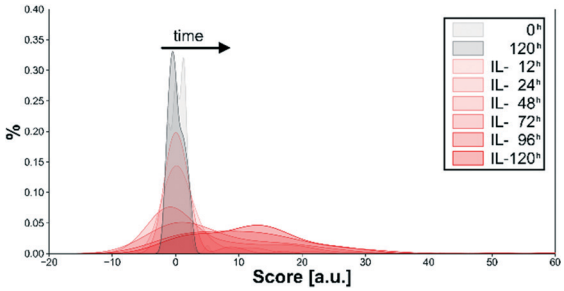

Fig. 4 Score outcome for CD56^{dim} of IL-15 investigations over IL treatment time (0–120 h). The higher the score value, the higher the probability of correct classification of a cell. A clear score shift for IL stimulation over time is noticed.

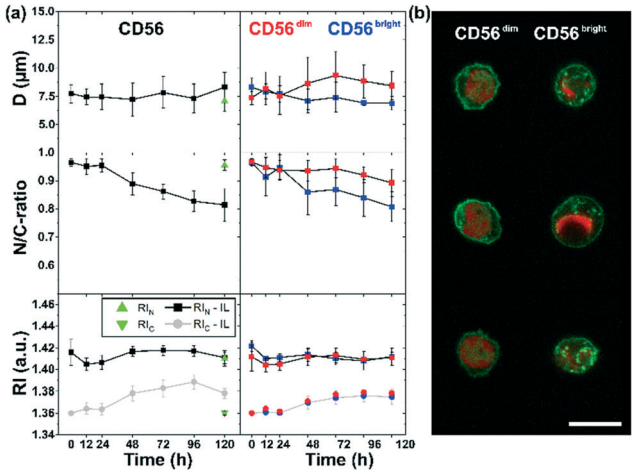

Fig. 5 Biophysical cell features during IL-15 investigation. (a) CD56 features (n = 286, 50, 74, 70, 66, 57 and 129), before and after ML classification for CD56^{dim} (n = 171, 26, 41, 38, 47, 52 and 119) and CD56^{bright} (n = 115, 24, 33, 32, 19, 5 and 10) for time 0 h, 12 h-IL, 24 h-IL, 48 h-IL, 72 h-IL, 96 h-IL and 120 h-IL respectively. Triangles indicate the control measurement at 120 h (n = 97) without IL-15 treatment. (b) Fluorescence images of CD56^{dim} and CD56^{bright} (green colour shows 'Wheat Germ Agglutinin', while red colour illustrates 'Sytox Green' staining). The length of the scale bar is 10 µm.

patient. Such blood samples result in an enriched NK cell fraction compared to that of physiological PBMCs, which allowed us to test our measurement approach for therapeutic purposes. We first analysed the mobilized sample with our measurement approach to retrieve biophysical features. Then, a ML classifier for PBMCs was trained on such data for the identification of the main classes of PBMCs (erythrocytes,[55] lymphocytes,[56] NK cells, and monocytes[51] with respectively n = 110, 200, 200 and 148 cells). Note that the PBMC classifier was trained for different cell classes using the same experimental setup as well as the same ML parameters as those for the NK classifier.

The morphometric based ML results indicate 25% lymphocytes and 75% NK cells in the mobilized cell sample and the absence of the other investigated cell classes, which is in good agreement with the flow cytometry outcomes, which show 78% NK cells (CD56 positive), 18% T-lymphocytes (CD3 positive) and 2% B-lymphocytes (CD19 positive) (see ESI† Fig. S5). Intriguingly, the flow cytometric analysis of the mobilized cells after IL-15 stimulation revealed a double population of NK lymphocytes (CD56 positive): a larger one (about 30% of the CD56 positive cells) and a smaller one (about 70% of CD56 positive cells). This data is consistent with the different morphological characteristics of the CD56^{dim} and CD56^{bright} cells.

After identification as lymphocytes, we classified the mobilized sample using the NK classifier (Fig. 3a). The biophysical cell features are reported as 3D scatter plots (and projected as 2D planes for each feature combination) to illustrate the morphological transition upon IL treatment. The results indicate the spreading of data clouds over time (indicating biophysical cell changes), especially after 48 h compared to the reference measurement (120 h without IL treatment). Moreover, we noticed that the NK cell classifier score for CD56^{dim} is low at time 0 h and significantly increases over time (see Fig. 4).

After 48 h, the CD56^{dim} score values significantly increase and demonstrate robust classification outcomes. The results indicate 60% CD56^{dim} cells and 40% CD56^{bright} cells at 0 h (see Fig. 3b). Such a proportion is different from those in the literature (see Table 1), where the high amount of CD56^{bright} can be ascribed to the mobilization with G-CSF.[71–74] The results show that the CD56^{dim} NK cell subclass increases in ratio over the CD56^{bright} ones over time (from 60 to 92%, see Fig. 3b), which illustrate the cell transition induced by IL-15. Fig. 5 (see ESI† Table S2) summarizes features from our approach over IL treatment time. The CD56 outcome indicates the biophysical features obtained from our measurement approach, while the CD56^{dim} and CD56^{bright} features are obtained after classification with the NK classifier. The results show a small reduction of cell dimensions for classified CD56^{bright} cells over time, while the CD56^{dim} dimensions increase. Also, the CD56^{bright} cells show a higher reduction of their N/C-ratio over time compared to the CD56^{dim} cells.

Moreover, RI$_N$ differences between CD56^{bright} and CD56^{dim} at 0 h decrease during IL treatment, while the RI$_C$ values significantly change, increasing from 1.36 to 1.38. Such variations can indicate that IL-15 affects the cytosolic compartment more than the nuclear one, promoting the

Table 1 Literature and experimental cell ratio values for CD56^{bright} *versus* CD56^{dim} NK cell subclasses. Experimental values are from four healthy probands with n = 187, 120, 74 and 114

CD56^{bright}	CD56^{dim}	Experiment/references
10%	90%	Ref. 6
≤10%	90%	Ref. 2
~10%	~90%	Ref. 3
16%	84%	Sample #1
25%	75%	Sample #2
22%	78%	Sample #3
38%	62%	Sample #4
~25%	~74%	Average of samples

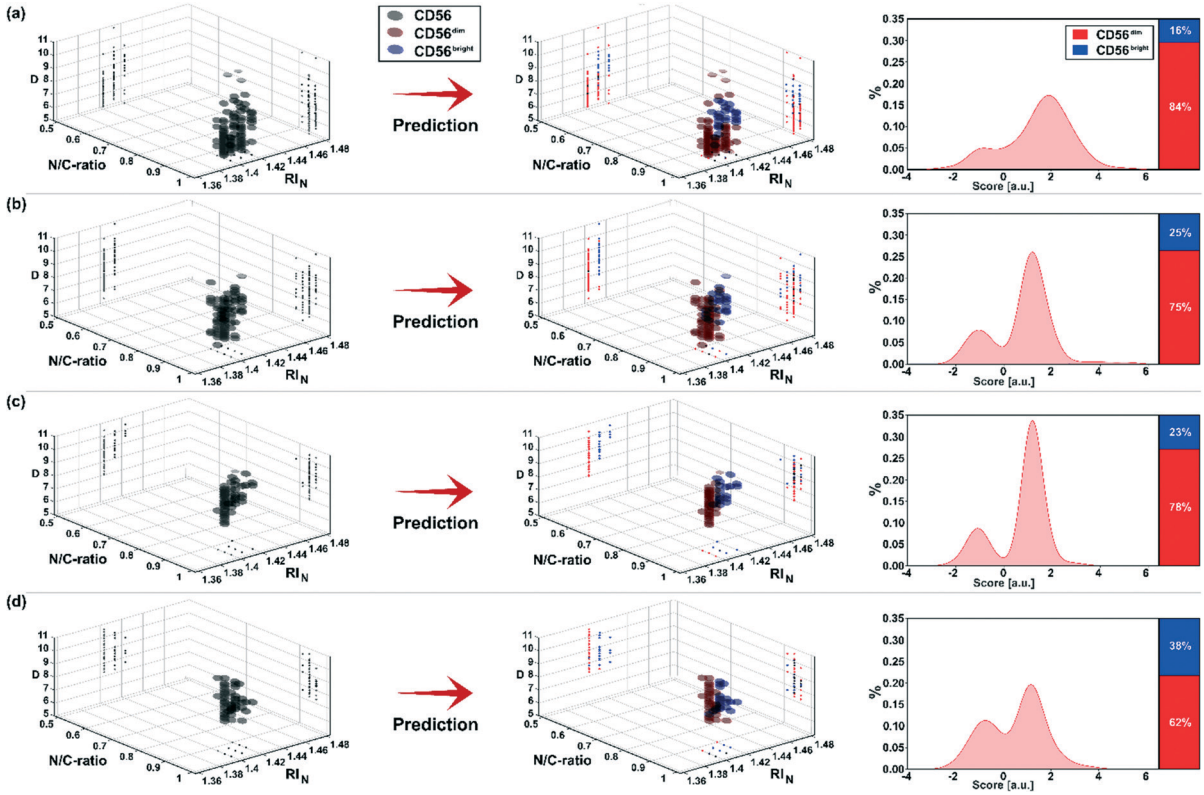

Fig. 6 NK cells from four probands are classified with the NK classifier (n = 187, 120, 74 and 114). The plots on the right indicate the score of the predicted CD56^{dim} subclass, where a higher score indicates stronger evidence for the prediction and *vice versa*. The numbering (a, b, c and d) on each row indicates the four different proband sample numbers (1, 2, 3 and 4).

possible formation of granules,[75] indicating a maturation towards the acquisition of cytotoxic ability. Note that the reference measurement (120 h without IL-15) remains constant with respect to the CD56^{bright} *versus* CD56^{dim} NK cell subclass ratio (see Fig. 3 and 5). Furthermore, as mentioned before, the results show that the N/C-ratio of cells significantly decreased, because of the cytosolic size increase, while the nucleus became more compact, probably due to a change in the state of transcription. To further confirm such outcomes, we performed immunofluorescence observations of IL-15 treated and untreated NK cells, staining both the cytosol and nucleus. As shown in Fig. 5, the cytosolic space appears denser after IL-15 stimulation with evident agglomerates.

Next, we applied the NK classifier to physiological cell samples (CD56), after purification from other cell classes (ESI† Fig. S5). We performed our measurements within 24 hours after blood donation. Biophysical features of the investigated cells were used as input for the ML classifier to retrieve the percentage of CD56^{bright} *versus* CD56^{dim} cells in each sample (see Fig. 3b). The NK classifier predicted significantly higher CD56^{dim} concentrations in the analysed samples. The overall average value of all four samples was respectively 25.25 ± 8.04% for CD56^{bright} NK cells and 74.75 ± 8.04% for CD56^{dim}. Fig. 6 shows the score values of the predicted cell classes for each of the four physiological samples. High (more positive) score values indicate correct cell classification. The results show a significantly higher score for CD56^{dim} compared to that for CD56^{bright}, with a higher prediction accuracy for CD56^{bright}. We noticed similar biophysical values for each analysed sample, showing CD56^{dim} majority with respect to CD56^{bright} (see Table 1). The slight discrepancies with literature data could be ascribed to the different measurement approaches (light scattering pattern *vs.* flow cytometry). Moreover, we investigated cells through bright-field microscopy observations and 'Trypan blue' tests before and after each measurement, demonstrating their viability (ESI† Fig. S4).

Conclusions

In this work, we propose an in-flow, non-invasive, label-free approach with supervised machine learning to classify subclasses (CD56^{bright} and CD56^{dim}) of human NK cells according to their biophysical features. This approach shows an overall classification accuracy of more than 86%, where CD56^{bright} NK cells are predicted with more than 94% accuracy. The microfluidic device used as a support for the single-cell light scattering analysis was optimized for ML training as well as for the classification of unknown samples. Moreover, we demonstrated for the first time that a ML

classifier is capable of discriminating $CD56^{bright}$ and $CD56^{dim}$ subclasses in NK cells.

We preliminarily tested our approach on NK cells after IL-15 treatment, showing the cytosolic compartment as the most relevant for NK cell subclass discrimination. We observed a significant change of cell dimensions for $CD56^{dim}$ and of the N/C-ratio for $CD56^{bright}$, as well as cytosolic compartment changes (RI_C) for $CD56^{dim}$ and $CD56^{bright}$ after IL-15 stimulation with a significant shift of $CD56^{bright}$ towards $CD56^{dim}$. Based on this, we succeeded in classifying NK cells from proband samples in accordance with cytometry tests with a majority of $CD56^{dim}$ with respect to $CD56^{dim}$. More importantly, viability tests confirmed that the use of appropriate microfluidic conditions and biocompatible fluids guarantees cell viability, demonstrating the non-invasiveness of the approach. By identifying NK cell subsets with high precision, our measurement approach could help in maximizing success in fundamental NK cell biology as well as quality control in cell therapy.

Author contributions

D. Dannhauser and D. Rossi conceived the project, performed experiments, and wrote the manuscript. D. Dannhauser developed the experimental setup. D. Rossi prepared cell samples and performed confocal investigations. A. T. Palatucci, V. Rubino, F. Carriero, G. Ruggiero and G. Terrazzano contributed to project design, performed experiments, and participated in manuscript writing. M. Ripaldi, M. Toriello and G. Maisto provided mobilized NK samples and were involved in project design. P. A. Netti supervised the project. F. Causa coordinated experimental activities and wrote the manuscript. All the authors reviewed the manuscript.

Conflicts of interest

There are no conflicts to declare.

Acknowledgements

This manuscript is dedicated to the memory of Prof. Ennio Carbone, an illustrious immunologist and scientist who sadly and prematurely passed away in March 2020. Prof. Carbone contributed significantly to the conception of this study and to the experimental design. We owe him immensely and he will always stay with us and in our thoughts.

We thank Mariarosaria Montagna, from Istituto per l'Endocrinologia e l'Oncologia Sperimentale "G. Salvatore", Consiglio Nazionale delle Ricerche, Naples 80131, Italy, for her technical help in cell sorting.

Notes and references

1 E. Vivier, S. Ugolini, D. Blaise, C. Chabannon and L. Brossay, Targeting natural killer cells and natural killer T cells in cancer, *Nat. Rev. Immunol.*, 2012, **12**, 239–252.

2 E. Carbone and G. Terrazzano, NK cells blur the frontier between innate and acquired immunity, *Front. Immunol.*, 2013, **3**, 400.

3 G. Terrazzano, M. Sica, C. Gianfrani, G. Mazzarella, F. Maurano, B. De Giulio, S. de Saint-Mezard, D. Zanzi, L. Maiuri, M. Londei, B. Jabri, R. Troncone, S. AuRIcchio, S. Zappacosta and E. Carbone, Gliadin regulates the NK-dendritic cell cross-talk by HLA-E surface stabilization, *J. Immunol.*, 2007, **179**, 372–381.

4 G. Terrazzano, V. Rubino, A. T. Palatucci, A. Giovazzino, M. Annunziatella, O. Vitagliano, F. Alfinito and G. Ruggiero, Natural killer expansion, human leukocyte antigens-E expression and CD 14+ CD 56+ monocytes in a myelodysplastic syndrome patient, *Eur. J. Haematol.*, 2013, **91**, 265–269.

5 S. Sivori, P. Vacca, G. Del Zotto, E. Munari, M. C. Mingari and L. Moretta, Human NK cells: surface receptors, inhibitory checkpoints, and translational applications, *Cell. Mol. Immunol.*, 2019, **16**, 430–441.

6 Y. He and T. Zhigang, NK cell education via nonclassical MHC and non-MHC ligands, *Cell. Mol. Immunol.*, 2017, **14**, 321–330.

7 L. E. Lowry and W. A. Zehring, Potentiation of natural killer cells for cancer immunotherapy: a review of literature, *Front. Immunol.*, 2017, **8**, 1061.

8 I. Langers, V. M. Renoux, M. Thiry, P. Delvenne and N. Jacobs, Natural killer cells: role in local tumor growth and metastasis, *Biol.: Targets Ther.*, 2012, **6**, 73.

9 M. A. Cooper, T. A. Fehniger and M. A. Caligiuri, The biology of human natural killer-cell subsets, *Trends Immunol.*, 2001, **22**, 633–640.

10 A. G. Freud, J. Yu and M. A. Caligiuri, Human natural killer cell development in secondary lymphoid tissues, *Semin. Immunol.*, 2014, **26**, 132–137.

11 A. G. Freud, B. L. Mundy-Bosse, J. Yu and M. A. Caligiuri, The broad spectrum of human natural killer cell diversity, *Immunity*, 2017, **47**, 820–833.

12 F. Galli, A. S. Rapisarda, H. Stabile, G. Malviya, I. Manni, E. Bonanno, G. Piaggio, A. Gismondi, A. Santoni and A. Signore, In vivo imaging of natural killer cell trafficking in tumors, *J. Nucl. Med.*, 2015, **56**, 1575–1580.

13 A. A. Maghazachi, Role of chemokines in the biology of natural killer cells, *The Chemokine System in Experimental and Clinical Hematology*, 2010, pp. 37–58.

14 J. E. Melsen, G. Lugthart, A. C. Lankester and M. W. Schilham, Human circulating and tissue-resident CD56bright natural killer cell populations, *Front. Immunol.*, 2016, **7**, 262.

15 A. Poli, T. Michel, M. Thérésine, E. Andrès, F. Hentges and J. Zimmer, CD56bright natural killer (NK) cells: an important NK cell subset, *Immunology*, 2009, **126**, 458–465.

16 M. A. Caligiuri, Human natural killer cells, *Blood*, 2008, **112**, 461–469.

17 B. Vanherberghen, P. E. Olofsson, E. Forslund, M. Sternberg-Simon, M. A. Khorshidi, S. Pacouret, K. Guldevall, M. Enqvist, K. J. Malmberg, R. Mehr and B. Önfelt,

Classification of human natural killer cells based on migration behavior and cytotoxic response, *Blood*, 2013, **121**, 1326–1334.

18 M. A. Cooper, M. Colonna and W. M. Yokoyama, Hidden talents of natural killers: NK cells in innate and adaptive immunity, *EMBO Rep.*, 2009, **10**, 1103–1110.

19 C. M. Tato, 21st century natural killers, *Nat. Rev. Immunol.*, 2019, **19**, 69.

20 I. Levi, H. Amsalem, A. Nissan, M. Darash-Yahana, T. Peretz, O. Mandelboim and J. Rachmilewitz, Characterization of tumor infiltrating natural killer cell subset, *Oncotarget*, 2015, **6**, 13835.

21 R. S. Mehta, B. Randolph, M. Daher and K. Rezvani, NK cell therapy for hematologic malignancies, *Int. J. Hematol.*, 2018, **107**, 262–270.

22 V. Bachanova and J. S. Miller, NK cells in therapy of cancer, *J. Environ. Pathol., Toxicol. Oncol.*, 2014, **19**, 1–2.

23 N. Sakamoto, T. Ishikawa, S. Kokura, T. Okayama, K. Oka, M. Ideno, F. Sakai, A. Kato, M. Tanabe, T. Enoki, J. Mineno, Y. Naito, Y. Itoh and T. Yoshikawa, Phase I clinical trial of autologous NK cell therapy using novel expansion method in patients with advanced digestive cancer, *J. Transl. Med.*, 2015, **13**, 1–13.

24 M. Cheng, Y. Chen, W. Xiao, R. Sun and Z. Tian, K cell-based immunotherapy for malignant diseases, *Cell. Mol. Immunol.*, 2013, **10**, 230–252.

25 H. Hujisaki, H. Kadkuda, N. Shimaski, C. Imai, J. Ma, T. Lockey, P. Eldridge, W. H. Leung and D. Capana, Expansion of highly cytotoxic human natural killer cells for cancer cell therapy, *Cancer Res.*, 2009, **69**, 4010–4017.

26 M. A. Geller, S. Cooley, P. L. Judson, R. Ghebre, L. F. Carson, P. A. Argenta, A. L. Jonson, A. Panoskaltsis-Mortari, J. Curtsinger, D. McKenna, K. Dusenbery, R. Bliss, L. S. Downs and J. S. Miller, A phase II study of allogeneic natural killer cell therapy to treat patients with recurrent ovarian and breast cancer, *Cytotherapy*, 2011, **13**, 98–107.

27 A. T. Björklund, M. Carlsten, E. Sohlberg, L. L. Liu, T. Clancy, M. Karimi, S. Cooley, J. S. Miller, M. Klimkowska, M. Schaffer, E. Watz, K. Wikström, P. Blomberg, B. Engelbrekt Wahlin, M. Palma, L. Hansson, P. Ljungman, E. Hellström-Lindberg, H. G. Ljunggren and K. J. Malmberg, Complete remission with reduction of high-risk clones following haploidentical NK-cell therapy against MDS and AML, *Clin. Cancer Res.*, 2018, **24**, 1834–1844.

28 M. J. Smyth, E. Cretney, J. M. Kelly, J. A. Westwood, S. E. A. Street, H. Yagita, K. Takeda, S. L. H. van Dommelen, M. A. Degli-Esposti and Y. Hayakawaa, Activation of NK cell cytotoxicity, *Mol. Immunol.*, 2005, **42**, 501–510.

29 J. Lieberman, The ABCs of granule-mediated cytotoxicity: new weapons in the arsenal, *Nat. Rev. Immunol.*, 2003, **3**, 361–370.

30 D. A. Vallera, M. Felices, R. McElmurry, V. McCullar, X. Zhou, J. U. Schmohl, B. Zhang, A. J. Lenvik, A. Panoskaltsis-Mortari, M. R. Verneris, J. Tolar, S. Cooley, D. J. Weisdorf, B. R. Blazar and J. S. Miller, IL15 trispecific killer engagers (TriKE) make natural killer cells specific to CD33+ targets while also inducing persistence, in vivo expansion, and enhanced function, *Clin. Cancer Res.*, 2016, **22**, 3440–3450.

31 M. J. Szczepanski, M. Szajnik, A. Welsh, K. A. Foon, T. L. Whiteside and M. Boyiadzis, Interleukin-15 enhances natural killer cell cytotoxicity in patients with acute myeloid leukemia by upregulating the activating NK cell receptors, *Cancer Immunol. Immunother.*, 2010, **59**, 73.

32 J. R. M. Van Audenaerde, J. De Waele, E. Marcq, J. Van Loenhout, E. Lion, J. M. J. Van den Bergh, R. Jesenofsky, A. Masamune, G. Roeyen, P. Pauwels, F. Lardon, M. Peeters and E. L. J. Smits, Interleukin-15 stimulates natural killer cell-mediated killing of both human pancreatic cancer and stellate cells, *Oncotarget*, 2017, **8**, 56968.

33 K. S. Campbell and J. Hasegawa, Natural killer cell biology: an update and future directions, *J. Allergy Clin. Immunol.*, 2013, **132**, 536–544.

34 Y. T. Bryceson, C. Fauriat, J. M. Nunes, S. M. Wood, N. K. Björkström, E. O. Long and H. G. Ljunggren, Functional analysis of human NK cells by flow cytometry, *Natural Killer Cell Protocols*, 2010, pp. 335–352.

35 M. Brown and C. Wittwer, Flow cytometry: principles and clinical applications in hematology, *Clin. Chem.*, 2000, **46**, 1221–1229.

36 H. T. Maecker, J. Philip McCoy Jr and the FOCIS Human Immunophenotyping Consortium, A model for harmonizing flow cytometry in clinical trials, *Nat. Immunol.*, 2010, **11**, 975.

37 K. A. Muirhead, P. K. Horan and G. Poste, Flow cytometry: present and future, *Nat. Biotechnol.*, 1985, **3**, 337–356.

38 J. Ford, Red blood cell morphology, *Int. J. Lab. Hematol.*, 2013, **35**, 351–357.

39 J. Prinyakupt and C. Pluempitiwiriyawej, Segmentation of white blood cells and comparison of cell morphology by linear and naïve Bayes classifiers, *Biomed. Eng. Online*, 2015, **14**, 1–19.

40 A. Merino, L. Puigví, L. Boldú, S. Alférez and J. Rodellar, Optimizing morphology through blood cell image analysis, *Int. J. Lab. Hematol.*, 2018, **40**, 54–61.

41 N. Tatsumi and R. V. Pierre, Automated image processing: past, present, and future of blood cell morphology identification, *Clin. Lab. Med.*, 2002, **22**, 299–315.

42 I. Kviatkovsky, A. Zeidan, D. Yeheskely-Hayon, E. L. Shabad, E. J. Dann and D. Yelin, Measuring sickle cell morphology during blood flow, *Biomed. Opt. Express*, 2017, **8**, 1996–2003.

43 N. Theera-Umpon and D. Sompong, Morphological granulometric features of nucleus in automatic bone marrow white blood cell classification, *IEEE Trans. Inf. Technol. Biomed.*, 2007, **11**, 353–359.

44 K. C. Lee, J. Guck, K. Goda and K. K. Tsia, Toward deep biophysical cytometry: prospects and challenges, *Trends Biotechnol.*, 2021, DOI: 10.1016/j.tibtech.2021.03.006.

45 Y. Li, C. M. Nowak, U. Pham, K. Nguyen and L. Bleris, Cell morphology-based machine learning models for human cell state classification, *npj Syst. Biol. Appl.*, 2021, **7**, 1–9.

46 A. Walsh, K. Mueller, I. Jones, C. M. Walsh, N. Piscopo, N. N. Niemi, D. J. Pagliarini, K. Saha and M. C. Skala,

Labelfree Method for Classification of T cell Activation, bioRxiv, 2019, DOI: 10.1101/536813.

47 D.-H. Lee, X. Li, N. Ma, M. A. Digman and A. P. Lee, Rapid and label-free identification of single leukemia cells from blood in a high-density microfluidic trapping array by fluorescence lifetime imaging microscopy, *Lab Chip*, 2018, **18**, 1349–1358.

48 M. Nassar, M. Doan, A. Filby, O. Wolkenhauer, D. K. Fogg, J. Piasecka, C. A. Thornton, A. E. Carpenter, H. D. Summers, P. Rees and H. Hennig, Label-Free Identification of White Blood Cells Using Machine Learning, *Cytometry, Part A*, 2019, **95**, 836–842.

49 A. Isozaki, J. Harmon, Y. Zhou, S. Li, Y. Nakagawa, M. Hayashi, H. Mikami, C. Lei and K. Goda, AI on a chip, *Lab Chip*, 2020, **20**, 3074–3090.

50 D. Kim, Y. Min, J. M. Oh and Y. K. Cho, AI-powered transmitted light microscopy for functional analysis of live cells, *Sci. Rep.*, 2019, **9**, 1–9.

51 M. Ugele, M. Weniger, M. Leidenberger, Y. Huang, M. M. Bassler, O. Friedrich, B. Kappes, O. Hayden and L. Richter, Label-free, high-throughput detection of P. falciparum infection in sphered erythrocytes with digital holographic microscopy, *Lab Chip*, 2018, **18**(12), 1704–1712.

52 M. Ugele, M. Weniger, M. Stanzel, M. Bassler, S. W. Krause, O. Friedrich, O. Hayden and L. Richter, Label-free high-throughput leukemia detection by holographic microscopy, *Adv. Sci.*, 2018, **5**(12), 1800761.

53 B. Kemper, H. Eilers, T. Klein, K. Brinker and S. Ketelhut, Quantitative phase imaging-based machine learning approaches for the analysis of adherent and suspended cells, in *Three-Dimensional and Multidimensional Microscopy: Image Acquisition and Processing XXVIII*, International Society for Optics and Photonics, 2021, vol. 11649, p. 116490B.

54 D. Dannhauser, G. Romeo, F. Causa, I. De Santo and P. A. Netti, Multiplex single particle analysis in microfluidics, *Analyst*, 2014, **139**, 5239–5246.

55 D. Dannhauser, D. Rossi, F. Causa, P. Memmolo, A. Finizio, T. Wriedt, J. Hellmers, Y. Eremin, P. Ferraro and P. A. Netti, Optical signature of erythrocytes by light scattering in microfluidic flows, *Lab Chip*, 2015, **15**, 3278–3285.

56 D. Dannhauser, D. Rossi, M. Ripaldi, P. A. Netti and F. Causa, Single-cell screening of multiple biophysical properties in leukemia diagnosis from peripheral blood by pure light scattering, *Sci. Rep.*, 2017, **7**, 12666.

57 D. Dannhauser, D. Rossi, P. Memmolo, A. Finizio, P. Ferraro, P. A. Netti and F. Causa, Biophysical investigation of living monocytes in flow by collaborative coherent imaging techniques, *Biomed. Opt. Express*, 2018, **9**, 5194–5204.

58 D. Rossi, D. Dannhauser, M. Telesco, P. A. Netti and F. Causa, CD4+ versus CD8+ T-lymphocyte identification in an integrated microfluidic chip using light scattering and machine learning, *Lab Chip*, 2019, **19**, 3888–3898.

59 T. B. Casale and M. A. Kaliner, Rapid method for isolation of human mononuclear cells free of significant platelet contamination, *J. Immunol. Methods*, 1982, **55**, 347–353.

60 C. S. Haas, Participação das proteínas morfogenéticas ósseas no crescimento folicular final, ovulação e função luteal, 2018, 119.

61 G. Terrazzano, S. Bruzzaniti, V. Rubino, M. Santopaolo, A. T. Palatucci, A. Giovazzino, C. La Rocca, P. de Candia, A. Puca, F. Perna, C. Procaccini, V. De Rosa, C. Porcellini, S. De Simone, V. Fattorusso, A. Porcellini, E. Mozzillo, R. Troncone, A. Franzese, J. Ludvigsson, G. Matarese, G. Ruggiero and M. Galgani, Type 1 diabetes progression is associated with loss of CD3+ CD56+ regulatory T cells that control CD8+ T-cell effector functions, *Nat. Metab.*, 2020, **2**, 142–152.

62 G. D'Avino, G. Romeo, M. M. Villone, F. Greco, P. A. Netti and P. L. Maffettone, Single line particle focusing induced by viscoelasticity of the suspending liquid: theory, experiments and simulations to design a micropipe flow-focuser, *Lab Chip*, 2012, **12**, 1638–1645.

63 G. Romeo, G. D'Avino, F. Greco, P. A. Netti and P. L. Maffettone, Viscoelastic flow-focusing in microchannels: scaling properties of the particle radial distributions, *Lab Chip*, 2013, **13**, 2802–2807.

64 D. Dannhauser, M. I. Maremonti, V. Panzetta, D. Rossi, P. A. Netti and F. Causa, Mechanical phenotyping of breast cell lines by in-flow deformation-dependent dynamics under tuneable compressive forces, *Lab Chip*, 2020, **20**, 4611–4622.

65 D. Dannhauser, G. Romeo, F. Causa and P. A. Netti, Small angle light scattering characterization of single micrometric particles in microfluidic flows, Optical Methods for Inspection, Characterization, and Imaging of Biomaterials, International Society for Optics and Photonics, 2013, vol. 8792.

66 P. J. Delves, S. J. Martin, D. R. Burton and I. M. Roitt, *Roitt's essential immunology*, John Wiley & Sons, 2017.

67 K. Roberts, B. Alberts, A. Johnson, P. Walter and T. Hunt, *Molecular biology of the cell*, Garland Science, New York, 2002.

68 N. I. C. Marzuki, N. H. Mahmood and M. A. A. Razak, Segmentation of white blood cell nucleus using active contour, *J. Teknol.*, 2015, **74**, 6.

69 R. A. Drezek, M. Guillaud, T. G. Collier, I. Boiko, A. Malpica, C. E. MacAulay, M. Follen and R. R. RIchards-Kortum, Light scattering from cervical cells throughout neoplastic progression: influence of nuclear morphology, DNA content, and chromatin texture, *J. Biomed. Opt.*, 2003, **8**, 7–16.

70 M. Golkaram, J. Jang, S. Hellander, K. S. Kosik and L. Petzold, The role of chromatin density in cell population heterogeneity during stem cell differentiation, *Sci. Rep.*, 2017, **7**, 1–11.

71 H. J. Kolb, J. Mittermüller, C. Clemm, E. Holler, G. Ledderose, G. Brehm, M. Heim and W. Wilmanns, Donor leukocyte transfusions for treatment of recurrent chronic myelogenous leukemia in marrow transplant patients, *Blood*, 1990, **76**, 2462–2465.

72 J. S. Miller, F. Prosper and V. McCullar, Natural killer (NK) cells are functionally abnormal and NK cell progenitors are

diminished in granulocyte colony-stimulating factor–mobilized peripheral blood progenitor cell collections, *Blood*, 1997, **90**, 3098–3105.

73 H. Tayebi, F. Kuttler, P. Saas, A. Lienard, B. Petracca, V. Lapierre, C. Ferrand, T. Fest, J. Y. Cahn, D. Blaise, M. Kuentz, P. Hervé, P. Tiberghien and E. Robinet, Effect of granulocyte colony-stimulating factor mobilization on phenotypical and functional properties of immune cells, *Exp. Hematol.*, 2001, **29**, 458–470.

74 Y. C. Su, S. C. Li, C. K. Hsu, C. C. Yu, T. J. Lin, C. Y. Lee and H. F. Liao, G-CSF downregulates natural killer cell-mediated cytotoxicity in donors for hematopoietic SCT, *Bone Marrow Transplant.*, 2012, **47**, 73–81.

75 W. E. Carson, J. G. Giri, M. J. Lindemann, M. L. Linett, M. Ahdieh, R. Paxton, D. Anderson, J. Eisenmann, K. Grabstein and M. A. Caligiuri, Interleukin (IL) 15 is a novel cytokine that activates human natural killer cells via components of the IL-2 receptor, *J. Exp. Med.*, 1994, **180**, 1395–1403.